Available online at www.sciencedirect.com

ScienceDirect

Nuclear Physics A 987 (2019) 128–143

NUCLEAR PHYSICS A

www.elsevier.com/locate/nuclphysa

Excitation function of the $^{nat}Ti(p,x)^{48}V$, $^{47,46,44m}Sc$ reactions within the energy range of 10-22 MeV

Siddharth Parashari [a,*], S. Mukherjee [a], B.K. Nayak [b], H. Naik [c], S.V. Suryanarayana [b], R. Makwana [a], N.L. Singh [a]

[a] *Department of Physics, The M. S. University of Baroda, Vadodara-390002, India*
[b] *Nuclear Physics Division, Bhabha Atomic Research Center, Mumbai-400085, India*
[c] *Radiochemistry Division, Bhabha Atomic Research Center, Mumbai-400085, India*

Received 1 December 2018; received in revised form 16 April 2019; accepted 18 April 2019
Available online 26 April 2019

Abstract

The production cross-sections of the ^{48}V, ^{47}Sc, ^{46}Sc, and ^{44m}Sc residues were measured in the proton induced ^{nat}Ti reactions using the stack foil activation technique followed by the off-line $\gamma - ray$ spectrometry. The present work was carried out at 14UD BARC-TIFR Pelletron accelerator, Mumbai, India. The proton beam of 22 MeV was used for the irradiation of the samples and was degraded along the stack of target foils using aluminum (Al) degraders. The measured cross-section data were compared with the existing literature data available in EXFOR data library. The results were also compared with the theoretical values from the TALYS-1.9 and the ALICE-2014 nuclear model codes using the suitable input level density models. The pre-equilibrium contribution has also been estimated for the populated reaction residues in the present work. The present work offers a comparison between the two theoretical model codes using a similar input level density model. The reaction product ^{44m}Sc also has some practical medical applications in nuclear medicine.

Keywords: $^{nat}Ti(p,x)$ reactions; Stack foil activation; Off-line $\gamma - ray$ spectrometry; TALYS-1.9; ALICE-2014; Pre-equilibrium emission

* Corresponding author.
E-mail addresses: siddharthparashri5@gmail.com (S. Parashari), sk.mukherjee-phy@msubaroda.ac.in (S. Mukherjee).

https://doi.org/10.1016/j.nuclphysa.2019.04.009
0375-9474/

1. Introduction

Nuclear data relevant to Accelerator Driven Sub-critical system (ADSs) and International Thermonuclear Experimental Reactor (ITER) are of prime interest in recent years. Precise proton and neutron induced reaction data are demanded for the dose estimation, swelling of the fuel palette, hydrogen and gamma production, radiation damage estimation etc. Titanium alloys have a number of properties which make them attractive structural material candidates for fusion and fast reactors such as; high strength-to-weight ratio, intermediate strength values, good fatigue and creep rupture properties, small modulus of elasticity, high electrical resistivity, heat capacity, low coefficient of thermal expansion etc. [1]. The key highlight of Ti alloys is the low long-term ($<$ 10 years after shutdown) residual radioactivity which is very much needed to decrease the nuclear waste production. Therefore, titanium based alloys have been proposed and were found suitable for the application in fast reactor first wall and blanket structures [2]. In a fusion reactor about 80% of the energy released by 14 MeV neutrons is transferred to the first wall, superconducting magnets and breeding blanket. Rest 20% of the energy is carried by highly energetic protons and alpha particles. Therefore, the proton induced reaction cross-section data becomes vital for the Ti and Ti based alloys. Due to other vast applications of Ti metal in aerospace and medical accelerator technologies, the reaction cross-section data need more attention to be measured precisely. The decay data for these applications are known with a greater accuracy, however, the reaction cross-sections data related to the reactor applications need optimization to reduce the uncertainties within 10-25 MeV proton energies. The accuracy of measured reaction cross-section data largely depends on the relative uncertainty of the monitor reaction used. Nuclear Level density parameter plays an important role at such higher projectile energies as a number of outgoing channels and reaction processes starts to contribute in the population of a specific residual isotope. The pre-equilibrium and direct reaction processes play a dominating role in this energy regime. Therefore, it is interesting to compare the results from a comparison, which have been made among the level density models incorporated in two different model codes, TALYS-1.9 [3] and ALICE-2014 [4,5], which uses the similar input level densities but follows a different modeling approaches.

Titanium is also a potential candidate for the production of medical radioisotopes, like; ^{43}Sc, ^{44}Sc, ^{47}Sc, and many more. Among all, the ^{44}Sc is the most interesting radioisotope for nuclear imaging using $\beta^{+}\gamma$ coincidences [6]. Furthermore, together with the ^{47}Sc, it could be used for a pre-therapeutic imaging. Moreover, the ^{47}Sc radionuclide shows a promising interest in the radio-immunotherapy [7] due to its suitable β^{-} emission. The radioisotope ^{46}Sc can be used as a labeled micro-sphere for the investigation of an increased number of myocardial blood flow measurements [8], a radio-tracer to analyze Lungs [9] and can also be used as a cosmogenic radionuclide for an investigation into the evolution history of chondrites after separation from their parent body [10]. On the other hand, the radioisotope ^{48}V can be used as an alternative to the ^{68}Ge for a routine transmission scanning in PET [11]. From the above discussion, we can say that, an accurate determination of the $^{nat}Ti(p,x)^{48}V$,^{47,46,44m} Sc nuclear reactions are vital for the field of the nuclear medicine, trace element analysis, radiation protection in space and on earth etc. The $^{nat}Ti(p,x)^{48}V$ reaction is also an ideal reaction as to be used as the monitor for the charged particle beam energy and intensity for a low energy particle accelerator or a medical cyclotron [12]. Therefore, precise measurements of the $^{nat}Ti(p,x)^{48}V$ reaction are necessary for various practical applications and for the charged particle activation analysis.

The precise measurement of the cross-sections and relative contribution from the different processes, like pre-equilibrium (PE) process, compound nucleus (CN) and direct reactions, into

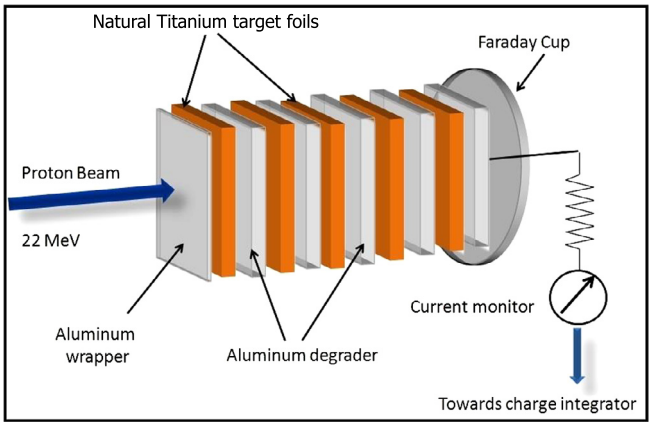

Fig. 1. (Color online.) The schematic diagram of the experimental setup of stacked foil activation technique.

the formation of radioisotopes for medical applications are also important for the production and the quality control of the medical isotopes. In general, the decay data for a particular isotope are known with a great accuracy, however, the reaction charged particle reaction cross-sections demands attention for the optimization and to develop new production routes. There can be various routes for the production of a specific medical isotope. Several authors [13–30] have investigated the (p,x) processes using natural or enriched Ti targets. A considerable amount of discrepancies were found among the existing data [31]. Therefore, the present work was aimed to reduce the existing discrepancies among the various literature data, which are vital for the charged particle activation analysis, monitor and production reaction cross-sections for different medical isotopes. The present work also offers a comparison between the nuclear model codes, TALYS-1.9 [3] and ALICE-2014 [4,5] using different suitable level density models present in both the codes.

2. Experimental details

The present measurement of the proton induced reaction cross-sections of ^{nat}Ti were carried out at 14UD Bhabha Atomic Research Center-Tata Institute of Fundamental Research (BARC-TIFR) Pelletron facility in Mumbai, India, by using the stack foil activation technique [32,33] followed by off-line $\gamma - ray$ spectroscopy. High purity ($\approx 99.98\%$) natural titanium (Ti) foils of thickness ≈ 12.7 μm were used as target. Aluminum foils of appropriate thickness were applied after each Ti target foil to reduce the proton beam energy significantly. The proton energy degradation on different targets along the stack was calculated by the SRIM code [34]. A schematic diagram of the stack used for the irradiation is presented in Fig. 1. The stack was wrapped in thin aluminum foil and kept inside the 6 meter irradiation port at the main beam line of the Pelletron. This port is most suitable for the high proton flux irradiation experiments. The proton beam was made to pass through a thick Ta collimator of 6 mm diameter to get a proper circular shaped beam. The irradiation of the stack was carried out for about 3 hours with a constant proton current of 180 nA to build up sufficient activity. The proton flux during the irradiation was calculated using the charge collected on a Faraday cup. In order to reduce the radioactive dose before recording the $\gamma - ray$ spectra, the irradiated samples were allowed to cool for few hours. Each sample was counted by using a pre-calibrated 80 cm^3 HPGe detector coupled to a PC based 4096 channel analyzers. The counting of the samples were carried out and was repeated over the

Table I
List of identified residues in the $p + ^{nat}Ti$ reactions with their spectroscopic data [35] and reaction threshold energies [36].

Nuclide	$T_{1/2}$	Decay mode (%)	E_γ (keV)	I_γ (%)	Channel	E_{th} (MeV)
^{48}V	15.97 days	ε(100%)	983.52	99.98	$^{47}Ti(p,\gamma)$	–
			1312.1	97.5	$^{48}Ti(p,n)$	4.8
					$^{49}Ti(p,2n)$	13.20
^{47}Sc	3.349 days	β^-(100%)	159.38	68.3	$^{48}Ti(p,2p)$	11.68
					$^{49}Ti(p,^3He)$	12.11
					$^{50}Ti(p,\alpha)$	2.28
^{46}Sc	83.79 days	β^-(100%)	889.28	99.98	$^{47}Ti(p,2p)$	10.69
			1120.55	99.99	$^{48}Ti(p,^3He)$	14.67
					$^{49}Ti(p,\alpha)$	1.98
					$^{50}Ti(p,n\alpha)$	13.13
^{44g}Sc	3.93 hours	ε(100%)	–	–	$^{47}Ti(p,\alpha)$	2.30
^{44m}Sc	58.61 hours	IT(98.8%)	271.1	86.7	$^{48}Ti(p,n\alpha)$	14.17
		ε(1.2%)				

period of time according to the half-life of the reaction products. The irradiated samples were placed at a distance of ≈5 cm from the detector end cap to avoid the pile-up effect and hence, to reduce the dead time of the detector. The HPGe detector was calibrated with a standard ^{152}Eu source. The resolution of the detector system during counting was measured as 1.82 keV at 1332 keV of ^{60}Co. The characteristic γ-lines with their respective half-lives were used to identify the residual nuclei of interest. All the spectroscopic data used in the present calculations were taken from NuDat [35] database, whereas the Q-values and the threshold energies were taken from Qtool [36], which are summarized in Table I.

3. Data analysis

The excitation function of the residues produced in the proton induced reactions with the natural Ti targets were measured at energies within the range of 10-22 MeV. The energy of the proton beam at the center of each target foil was calculated by SRIM code [34] and were found to be 21.95 ± 0.05, 19.84 ± 0.05, 17.56 ± 0.06, 15.05 ± 0.07, and, 12.94 ± 0.07 MeV, respectively. In the present case of study, four reaction products; ^{48}V, ^{47}Sc, ^{46}Sc, and ^{44m}Sc, were found to be produced in the $p + ^{nat}Ti$ reaction. The details related to the spectroscopic data which were used for the present analysis are presented in Table I. A typically recorded spectrum from the Ti foil irradiated around 19 MeV protons is shown in Fig. 2, with all the marked γ-ray peaks which were taken under consideration for the calculation of the cross-sections. As can be seen from the Table I, that the residue ^{48}V ($t_{1/2} = 15.97$ days) [35] can be produced through three different channels $^{47}Ti(p,\gamma)$, $^{48}Ti(p,n)$, and $^{49}Ti(p,2n)$ depending on the respective reaction threshold values. The counting statistics of the two strong γ-rays 983.52 (99.98%) and 1312.1 keV (97.5%) [35] were used separately for the measurement of the production cross-section of the ^{48}V. A weighted average was then calculated for the final cross-section of the $^{nat}Ti(p,x)^{48}V$ reactions. Similarly, the production cross-sections were measured for the ^{47}Sc and ^{46}Sc reaction residues. The contributing reaction channels from different isotopes of Ti into the ^{47}Sc and ^{46}Sc residues are listed in Table I. The residual nuclei ^{44}Sc have both the ground (3.97 hours) and the metastable (58.61 hours) [35] states. The relatively long half-life of the metastable state ^{44m}Sc

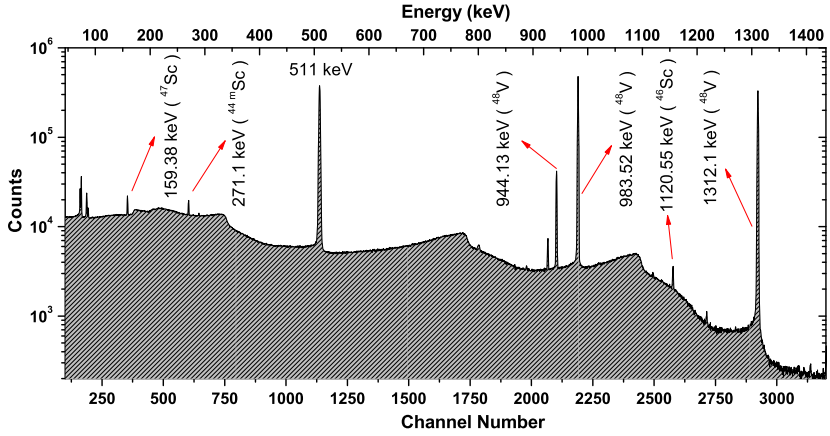

Fig. 2. (Color online.) A typical γ-ray energy spectrum obtained from the interaction of $p +^{nat} Ti$ at $E_{Lab} \approx 19$ MeV.

allowed us to cool the targets for a longer time for the spectra recording. The counting statistics of the 271.1 keV (86.7%) [35] γ-ray was used to measure the production cross-section of the ^{44m}Sc, which was found to be populated through the $^{47}Ti(p,\alpha)$ and $^{48}Ti(p,n\alpha)$ reaction channels.

The photo-peak counts from each γ-lines described above were used to calculate the reaction cross-sections for each residue by using the following expression,

$$\sigma_R = \frac{C_{obs}(C_L/L_T)\lambda}{N_0 \epsilon I_\gamma \phi K (1 - e^{-\lambda T_i})(e^{-\lambda T_c})(1 - e^{-\lambda T_{LT}})} \tag{1}$$

where, σ_R is the reaction cross-section, C_{obs} is the photo peak counts of the γ-line of interest, C_L, L_T are the clock time and the live time for the counting of the spectrum, λ is the decay constant, I_γ is the branching ratio for each $\gamma - ray$ taken from Ref. [35], N_0 is the total number of target nuclei in the sample, ϵ is the detector efficiency and ϕ is the proton flux. $K = [1 - exp(-\mu d)]/(\mu d)$ is the correction factor for the self-absorption of γ-rays in the sample thickness 'd' with the absorption coefficient μ.

4. Theoretical framework

4.1. Theoretical calculations by using the TALYS-1.9 code

The excitation function of the $^{nat}Ti(p,x)^{48}V,^{47,46,44m}Sc$ reactions were calculated as a function of incident particle energies by using the TALYS-1.9 model code [3]. The code is being used worldwide for the nuclear reaction cross-section data prediction. It can successfully reproduce the nuclear reaction cross-section, and the other data for the light particles (γ, n, p, α, and d etc.) induced reactions on incident particle energies up to 200 MeV. TALYS-1.9 code takes the input reaction parameters from the Reference Input Parameter Library (RIPL) database [37]. The code accommodates various reaction mechanisms like; compound nucleus, pre-equilibrium, and the direct reactions. It also incorporates the effects of level density as a function of incident particle energy. TALYS-1.9 is equipped with the optical model parameters by using a global potential proposed by Koning and Delaroche [38]. The Hauser-Feshbach model [39] takes care of the compound nuclear reaction using the exciton model developed by Kalbach [40] and is used to accommodate the pre-equilibrium contribution. TALYS consists of six level density models

(ldmodel 1-6) which can be used for the better description of the nuclear data. The level density models are; Constant Temperature Fermi gas model (CTFGM) [41], Back-shifted Fermi gas model (BSFGM) [42], Generalized superfluid model (GSFM) [43,44], Microscopic level densities from Goriely's and Hilaire's tables [45] and Microscopic level densities (temperature dependent HFB, Gogny force) [46], respectively.

The expression for the nuclear level density parameter 'a' including the shell effects can by given by the equation,

$$a = \tilde{a}\left(1 + \delta W \frac{1 - exp[-\gamma U]}{U}\right) \tag{2}$$

where, $\tilde{a}$ is the asymptotic level density value in the absence of any shell effects, γ is the damping parameter and δW is the shell correction energy. The Asymptotic value $\tilde{a}$ and the damping parameter can be given by,

$$\tilde{a} = \alpha A + \beta A^{2/3} \tag{3}$$

$$\gamma = \frac{\gamma_1}{A^{1/3}} + \gamma_2 \tag{4}$$

Different level density models can be invoked either by the "ldmodel" keyword or by changing the values of α, β and γ_1. The later gives a better control over the fitting of the reaction data. The single particle level density parameter 'g' (MeV^{-1}) is given by $g = A/K_{ph}$. Where K_{ph} is a constant and uses a default value 15.

4.2. Theoretical calculations by using the ALICE-2014 code

The excitation function of the $^{nat}Ti(p,x)^{48}V, ^{47,46,44m}Sc$ as a function of incident particle energies were also calculated by using the ALICE-2014 [4,5] model code. The code is based on the Hybrid Monte-Carlo Simulation (HMS) pre-compound decay [47], Weisskopf-Ewing evaporation [48], Bohr-Wheeler [49] fission models and the linear momentum conservation model of Chadwick and Oblozinsky [50] was used to incorporate the angular distribution. ALICE-2014 is based on the Monte Carlo simulation technique to reproduce the reaction data. The code can perform the theoretical calculations for the light as well as heavy-ion induced reactions flawlessly up to 250 MeV. The code mainly uses four level densities such as Fermi gas, backshifted pairing energies, Kataria-Ramamurthy and Obninsk. The level density model and the particle level density parameter (PLD), both can be changed in order to get the most significant fit for the experimental data. The PLD in ALICE-2014 may be calculated as, $a_{PLD} = A/K$, where A is the mass number of the composite nucleus and K is an adjustable parameter [51] (default value 9), which can be varied to match the excitation function of a particular reaction.

In the present work, the experimental data were compared by the cross-sections reproduced by activating different level density models (ldmodel 1-6) [41–46] present in TALYS-1.9 [3]. The present data were also compared with the theoretical predictions from ALICE-2014 [4,5] using the Fermi Gas, Kataria-Ramamurthy and Obninsk level density models. The level density parameter (PLD) was set as 9, which is set as default for each level density model in the ALICE-2014 [4,5] model code. It was seen from the previous data compilation, that the similar level density models in different nuclear model codes give rise to different cross-section data, therefore, a comparison among different level density models from TALYS-1.9 [3] and ALICE-2014 [4,5] is also presented.

Table II
Measured reaction cross-sections of the radionuclide produced in the $^{nat}Ti(p,x)$ reaction.

Energy (MeV)	Cross-Section (mb)			
	^{48}V	^{47}Sc	^{46}Sc	^{44m}Sc
21.95 ± 0.05	67.76 ± 5.83	10.79 ± 0.83	5.49 ± 0.45	3.54 ± 0.23
19.84 ± 0.05	93.46 ± 8.91	6.96 ± 0.52	4.22 ± 0.34	1.35 ± 0.09
17.56 ± 0.06	158.34 ± 14.23	2.98 ± 0.18	3.43 ± 0.22	1.42 ± 0.11
15.05 ± 0.07	328.54 ± 28.31	1.18 ± 0.08	2.09 ± 0.16	1.03 ± 0.08
12.94 ± 0.07	457.92 ± 42.44	1.06 ± 0.07	1.58 ± 0.12	0.84 ± 0.07

5. Results and discussion

In the present work, the excitation function of the $^{nat}Ti(p,x)^{48}V, ^{47,46,44m}Sc$ reactions have been measured at five proton energies of 21.95 ± 0.05, 19.84 ± 0.05, 17.56 ± 0.06, 15.05 ± 0.07, and, 12.94 ± 0.07 MeV, respectively. The measured cross-section for all the residues at different incident proton energies are summarized in Table II. The uncertainties in the present measurements were obtained as the quadratic sum of both statistical and systematic uncertainties. The statistical error in the present measurement was estimated to be $< 5\%$, which was reduced to this limit by performing the counting of each sample for a significant time. There could be various sources for the systematic uncertainty in the measured cross-sections. The fluctuations in the beam current result in the uncertainty in the incident flux. Therefore, the current was kept constant during the irradiation, and the error due to the flux was estimated to be $< 2\%$. The estimation of the foil thickness, weight of the foil and the relative error in the atomic mass of the sample may lead to the uncertainty in determining the number of target nuclei and comes out to be $< 3\%$. The uncertainty due to the finite size of the samples may appear in the efficiency of the detector and it is found to be $< 2\%$. The dead time of the HPGe detector was kept $< 1.5\%$ by keeping the sample effectively far from the detector endcap. Thus, the overall errors in the present measurements have been estimated as the quadratic sum of both statistical and systematic uncertainties and were found to be $< 10\%$.

5.1. Excitation function of the $^{nat}Ti(p,x)^{48}V$ reaction

The excitation function of the $^{nat}Ti(p,x)^{48}V$ reaction was measured at five incident proton energies, 21.95 ± 0.05, 19.84 ± 0.05, 17.56 ± 0.06, 15.05 ± 0.07, and, 12.94 ± 0.07 MeV and compared with the literature data [16–18,21–26,28], TALYS-1.9 [3] and the ALICE-2014 [4,5] nuclear model codes. Fig. 3 represents the comparison among the present results, the literature data and the theoretical reproduction of the cross-sections by using the different level density models (ldmodel 1-6) [41–46] presented in the TALYS-1.9 model code. On the other hand, Fig. 4 presents the comparison among the theoretical data using the Fermi Gas and Kataria-Ramamurthy level density models of ALICE-2014 with TALYS-1.9 default (Fermi Gas model), present results and the literature data. It can be observed from figure 3 that the measured data are in accord with the literature data for the entire range of the incident particle energies under consideration. The TALYS-1.9 input level density models were also find successful in order to reproduce the reaction data except the ldmodel 6 which was found to under-predict the data for the 6-14 MeV proton energies. On the other hand, we can observe from the Fig. 4 that the ALICE-2014 model code was found to over-predicting the reaction cross-section data by using

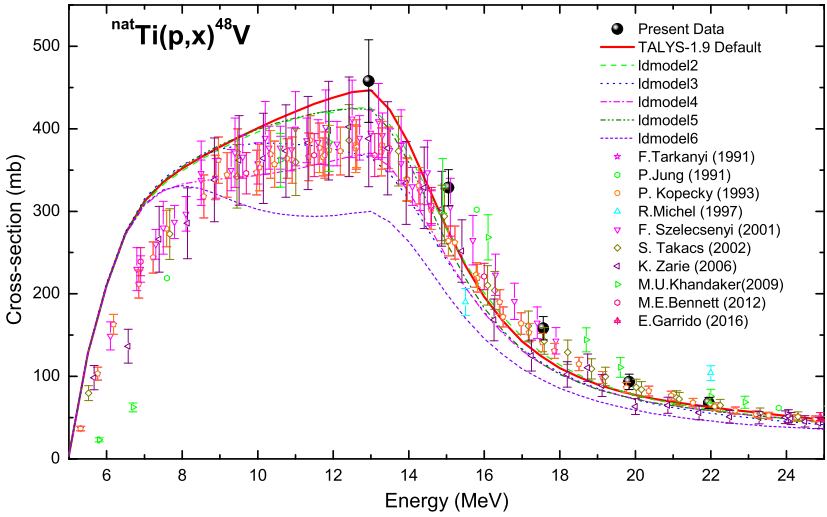

Fig. 3. (Color online.) Excitation function of $^{nat}Ti(p,x)^{48}V$ reaction. The comparison of the present and the literature data [16–18,21–26,28] with different level density model parameters (ldmodel 1-6) [41–46] in TALYS-1.9 [3].

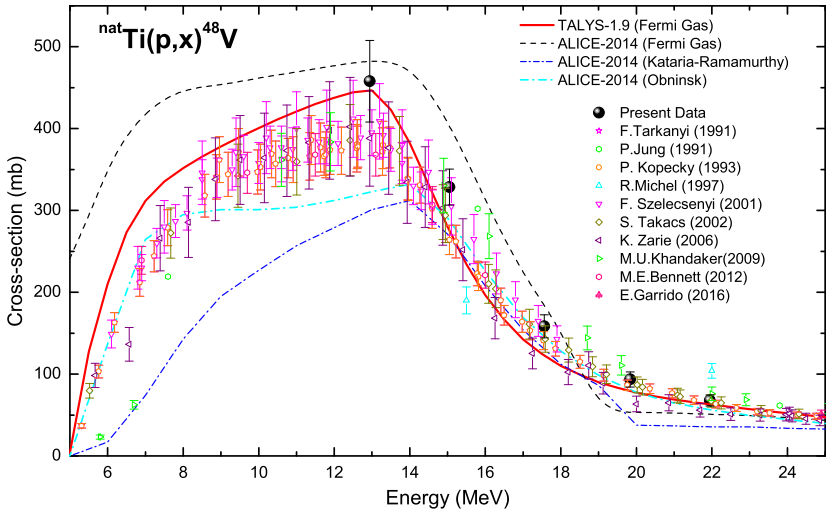

Fig. 4. (Color online.) Excitation function of $^{nat}Ti(p,x)^{48}V$ reaction. The comparison of the present and the literature data [16–18,21–26,28] with different level density model parameters (Fermi Gas and Kataria-Ramamurthy) in ALICE-2014 [4,5] and TALYS-1.9 [3] default values.

the similar Fermi Gas model as that of TALYS-1.9. However, the Kataria-Ramamurthy level density model was found to under-predict the cross-section data for the incident proton energies from threshold to 14 MeV. Moreover, the Obninsk level density model predicted the cross-section data up to an acceptable degree. The difference between the ALICE-2014 and TALYS-1.9 data values using different level density models may be attributed to the different level density parameter values has been set as default in both the codes.

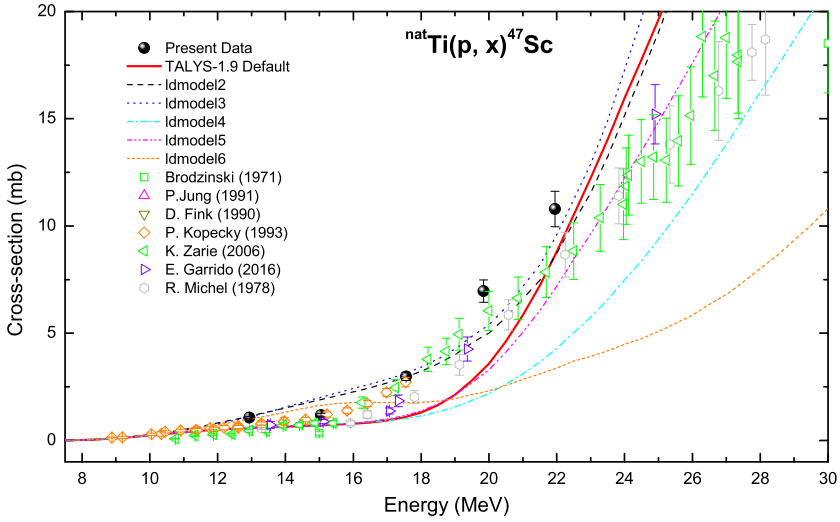

Fig. 5. (Color online.) Excitation function of $^{nat}Ti(p,x)^{47}Sc$ reaction. The comparison of the present and the literature data [14–17,19,24,28] with different level density model parameters (ldmodel 1-6) [41–46] in TALYS-1.9 [3].

5.2. Excitation function of the $^{nat}Ti(p,x)^{47}Sc$ reaction

The excitation function of the $^{nat}Ti(p,x)^{47}Sc$ reaction is plotted and compared with the literature data and the TALYS-1.9 [3] model code reproductions in Fig. 5. It can be observed from the figure that the present results offer minimal uncertainties as compared to the literature data [14–17,19,24,28] and were found to be in agreement with the previous findings. Fig. 5 also shows that the TALYS-1.9 level density model (ldmodel 1-5) [41–45] codes were found successful in order to reproduce the trend of the experimental data for the energy range under consideration except the ldmodel 6, which was found to under-predict the data for the incident particle energies above 20 MeV. Fig. 6 present the comparison between the TALYS-1.9 and ALICE-2014 model code reproductions using the Fermi Gas, Obninsk and Kataria-Ramamurthy level density models. A similar kind of trend can be observed for the Obninsk level density data values. The Fermi Gas model from both the codes was found to reproduce the reaction cross-section data successfully for the energy range under consideration, however, similar to the previous case, the Kataria-Ramamurthy level density predictions depart from the experimental data and continues under-predicting the data values above 18 MeV proton energies.

5.3. Excitation function of the $^{nat}Ti(p,x)^{46}Sc$ reaction

The measured excitation function of the $^{nat}Ti(p,x)^{46}Sc$ reaction are plotted and compared with the literature data, TALYS-1.9 and ALICE-2014 model codes in Fig. 7 and 8. The present results were found in accord with the literature data [14,16,25,27,28]. It can be seen from the Fig. 7 that there is a minor discrepancy between the data from Khandaker et al. [25] and Hermanne et al. [27], which may arise due to the utilization of the different monitor cross-sections for the flux calculations. It can also be seen that the uncertainties in the literature data significantly larger than the present data findings. The TALYS-1.9 and ALICE-2014 codes were found successful in order to reproduce the trend of the cross-section data for the entire range of the

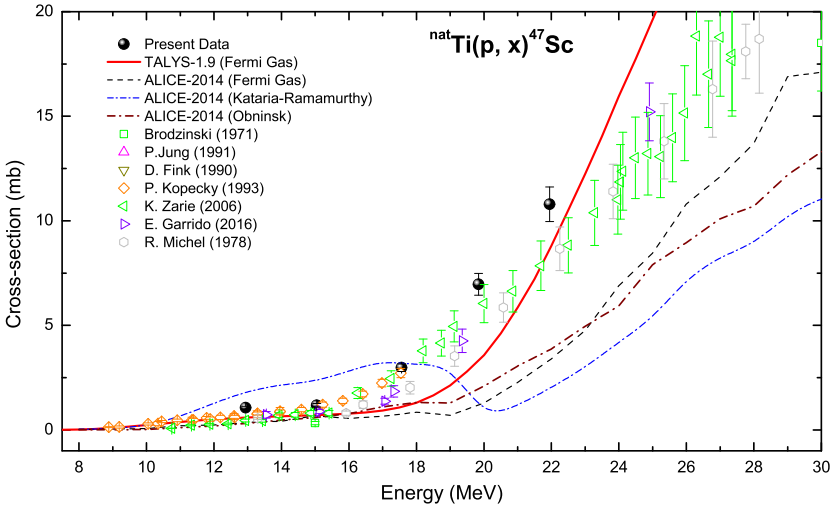

Fig. 6. (Color online.) Excitation function of $^{nat}Ti(p,x)^{47}Sc$ reaction. The comparison of the present and the literature data [14–17,19,24,28] with different level density model parameters (Fermi Gas and Kataria-Ramamurthy) in ALICE-2014 [4,5] and TALYS-1.9 [3] default values.

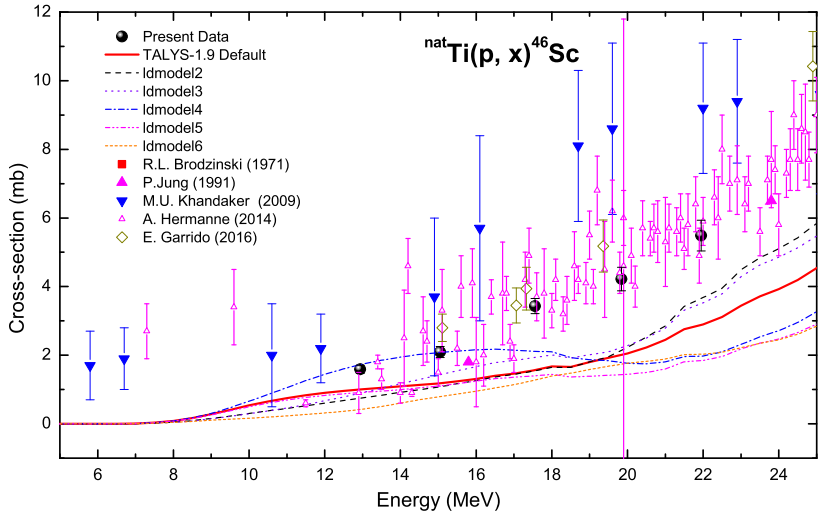

Fig. 7. (Color online.) Excitation function of $^{nat}Ti(p,x)^{46}Sc$ reaction. The comparison of the present and the literature data [14,16,25,27,28] with different level density model parameters (ldmodel 1-6) [41–46] in TALYS-1.9 [3].

incident particle energies under consideration. Furthermore, the ALICE-2014 values starts to decrease around 15 MeV and again increases significantly as the $^{48}Ti(p,^3He)$ channel starts to contribute. However, this trend is absent in TALYS-1.9 data values and experimental data.

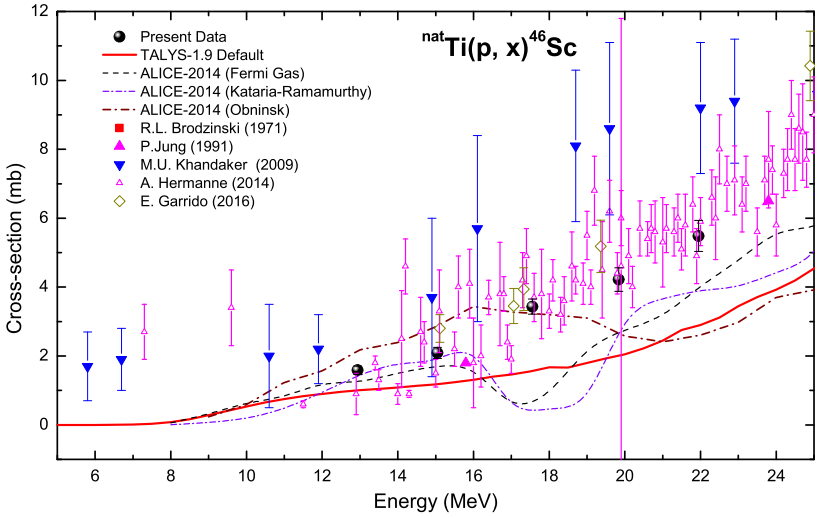

Fig. 8. (Color online.) Excitation function of $^{nat}Ti(p,x)^{46}Sc$ reaction. The comparison of the present and the literature data [14,16,25,27,28] with different level density model parameters (Fermi Gas and Kataria-Ramamurthy) in ALICE-2014 [4,5] and TALYS-1.9 [3] default values.

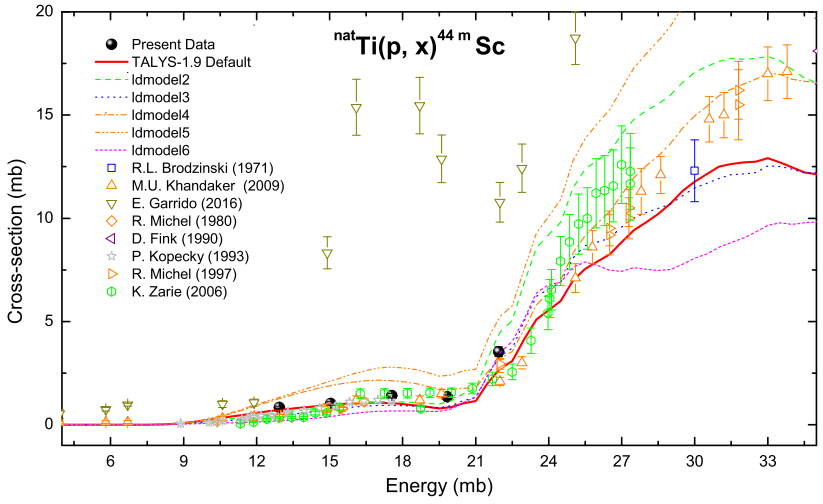

Fig. 9. (Color online.) Excitation function of $^{nat}Ti(p,x)^{44m}Sc$ reaction. The comparison of the present and the literature data [14,15,17,18,20,24,25,28] with different level density model parameters (ldmodel 1-6) [41–46] in TALYS-1.9 [3].

5.4. Excitation function of the $^{nat}Ti(p,x)^{44m}Sc$ reaction

The excitation function of the $^{nat}Ti(p,x)^{44m}Sc$ reaction are plotted in Figs. 9 and 10. The present results were also compared with the literature data [14,15,17,18,20,24,25,28], TALYS-1.9 [3] and the ALICE-2014 [4,5] model codes. It can be seen from the Fig. 9 that the present data is in a good agreement with the literature data and the data reproduced using different level density model codes in TALYS-1.9. It can also be seen from the Fig. 9 that the data from Gar-

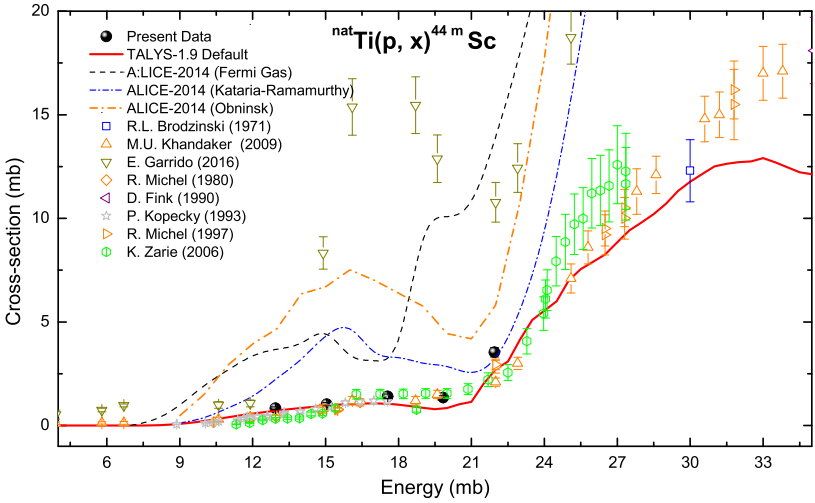

Fig. 10. (Color online.) Excitation function of $^{nat}Ti(p,x)^{44m}Sc$ reaction. The comparison of the present and the literature data [14,15,17,18,20,24,25,28] with different level density model parameters (Fermi Gas and Kataria-Ramamurthy) in ALICE-2014 [4,5] and TALYS-1.9 [3] default values.

rido et al. [28] do not follow the general trend of the cross-sections. On the other hand, Fig. 10 shows the comparison of the present results with the data reproduced using the ALICE-2014 code. It can be stated that the level density models present in ALICE-2014 [4,5] were found to be unsuccessful in order to reproduce the cross-section data. However, the predicted cross-sections were found to have an enhancement at two places; around 14 MeV and above 22 MeV proton energies. These enhancements in the predicted data may be attributed to the opening of the $^{48}Ti(p,n\alpha)$ ($E_{th} = 14.17$ MeV) and $^{49}Ti(p,2n\alpha)$ ($E_{th} = 22.47$ MeV) reaction channels, respectively. The further increasing trend of the cross-section is due to the involvement of the $^{50}Ti(p,3n\alpha)$ ($E_{th} = 33.63$ MeV) reaction in the production of the ^{44m}Sc radionuclide.

Since a considerable fraction of pre-equilibrium (PE) was found in the formation of product nuclei in the previous works [32,33] within 10-20 MeV projectile energies, therefore, to further investigate the role of PE process over the compound nucleus (CN) reaction process in the formation of different radioisotopes in the present work, theoretical reaction cross-sections have been calculated using the TALYS-1.9 code by taking only pure CN and both CN+PE processes into input description, separately. A comparison of the theoretical results with the present data have been shown in Fig. 11. It can be seen from the figure that a significant contribution is coming from the PE process into the production of the ^{48}V, ^{47}Sc, and ^{46}Sc radioisotopes. However, the CN description was found more satisfactory for the product nucleus ^{44m}Sc. In the view of the above discussion, PE contribution (PE %) has been calculated for the ^{48}V, ^{47}Sc, and ^{46}Sc residues as a function of projectile energy. The PE fraction (PE %) can be defined as the ratio of the PE cross-section to the evaporation residue (CN) cross-section. The results have been plotted in Fig. 12. The PE contribution was found to increase in general with the projectile energy. It can also be found from the figure that the PE fraction starts to saturate/die out for ^{48}V and ^{46}Sc residues as the $^{50}Ti(p,3n)$ and $^{48}Ti(p,2pn)$ channels open up around 23 MeV proton energies. However, the PE fraction completely dies out for ^{46}Sc at the opening up of $^{49}Ti(p,2pn)$ channel around 20 MeV. A comparison of the PE fractions among the $^{93}Nb(p,n)$ [32], $^{nat}Ag(p,n)$ [33] and $^{nat}Ti(p,n)$ (present work) reactions have also been shown in Fig. 13. It is evident from the

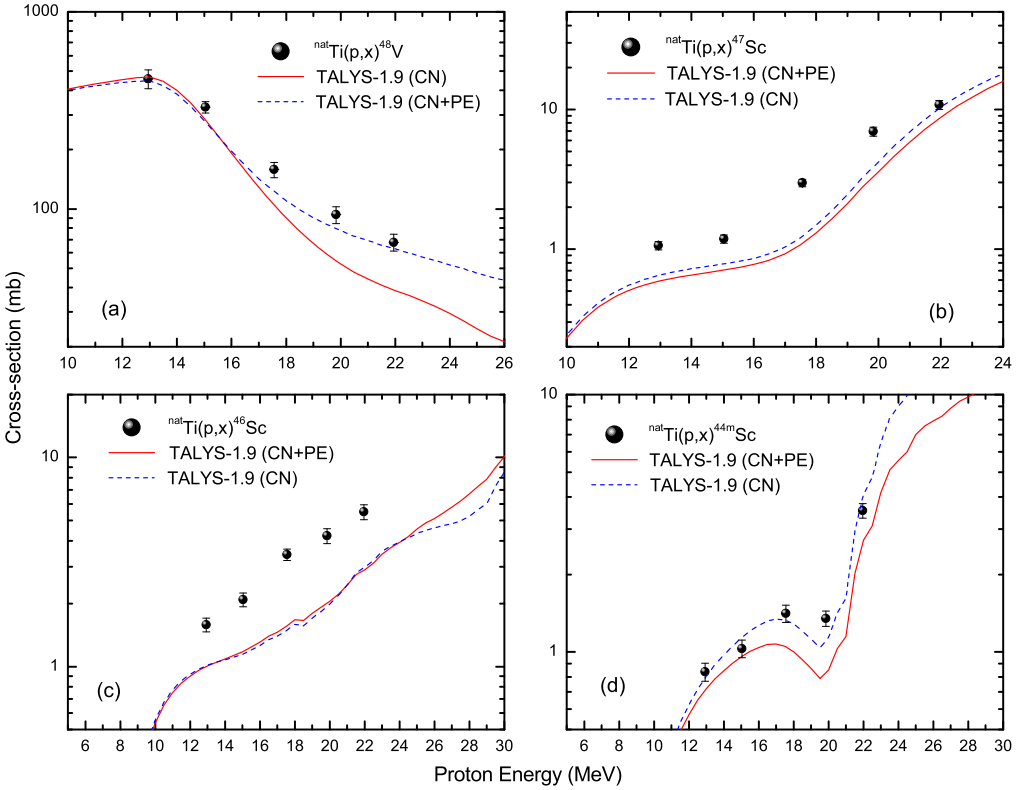

Fig. 11. (Color online.) The comparison of the excitation function of the (a) $^{nat}Ti(p,x)^{48}V$, (b) $^{nat}Ti(p,x)^{47}Sc$, (c) $^{nat}Ti(p,x)^{46}Sc$, and (d) $^{nat}Ti(p,x)^{44m}Sc$ reactions in the present work with pure CN and CN+PE cross-sections from TALYS-1.9 [3].

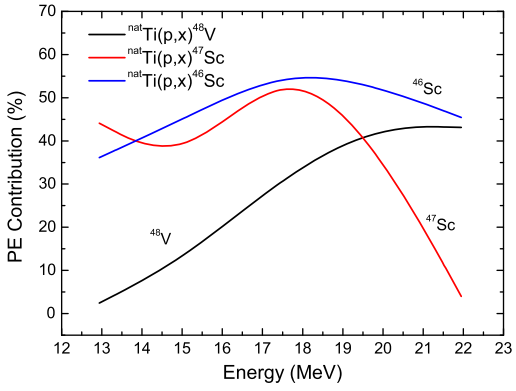

Fig. 12. (Color online.) The estimated PE contribution (PE%) from the present data as a function of projectile energy.

figure that the PE fraction depends on the associated Q-value of the reaction and decreases as with the increment in the $|Q|$-value.

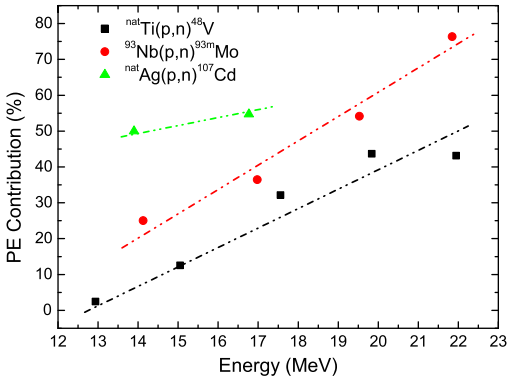

Fig. 13. (Color online.) A comparison of the estimated PE contribution (PE %) as a function of projectile energy in the production of radioisotopes in reactions with ^{nat}Ti, ^{93}Nb, and ^{nat}Ag through (p, n) channel (dotted lines are used to guide the eye).

6. Conclusions

In the present work, the excitation function of the $^{nat}Ti(p,x)$ reactions were measured at five incident proton energies 21.95 ± 0.05, 19.84 ± 0.05, 17.56 ± 0.06, 15.05 ± 0.07, and, 12.94 ± 0.07 MeV respectively. Four radionuclides, ^{48}V, ^{47}Sc, ^{46}Sc, and ^{44m}Sc were found to be populated in the present experiment. The present results were compared with the literature data and were found to be in a good agreement. The uncertainties were reduced below $< 10\%$ in the present analysis. Among the two codes, the TALYS-1.9 model code, in general, was found to be successful in order to reproduce the cross-section data to an acceptable degree for the entire range of the incident particle energies under consideration. On the other hand, ALICE-2014 model code was found to under/over-predict the data in case of the ^{48}V and ^{44m}Sc residues. The difference among the reproduced cross-section values from the TALYS-1.9 and ALICE-2014 model codes may be attributed to the different single particle level density parameter values set as default ($K_{ph} = 15$ in TALYS-1.9 and $a = 9$ in ALICE-2014) in both the codes. A significant contribution from the pre-equilibrium process has been found in the formation of radio-nuclides. The PE fraction was also found to be greater in the reaction with a lower associated Q-value and tend to increase with the proton energies.

Acknowledgements

One of the authors (SM) thanks to the DAE-BRNS for the sanction of a major research project (Sanction Number: 36(6)/14/22/2016-BRNS) as well as providing fellowship to the author (SP). The authors are thankful to Prof. V. Nanal and the staff of the Pelletron facility TIFR, Mumbai for their excellent operation of the accelerator and other supports during the experiment. The authors are also thankful to Dr. G. F. Steyn (iThemba Lab South Africa) for providing ALICE-2014 calculations.

References

[1] D.R. Harries, Ferritic martensitic steels for use in near term and commercial fusion reactors, in: Proceedings of the Topical Conference on Ferritic Alloys for Use in Nuclear Energy Technologies, Snowbird, Utah, June 19-23, 1983.

[2] J.W. Davis, D.L. Smith, J. Nucl. Mater. vols. 85 & 86 (1979) 71.
[3] A.J. Koning, S. Hilaire, S. Goriely, TALYS User Manual, a Nuclear Reaction Program, NRG-1755 ZG PETTEN, the Netherlands, 2015.
[4] M. Blann, Phys. Rev. Lett. 27 (1971) 337.
[5] M. Blann, Phys. Rev. Lett. 28 (1972) 757.
[6] C. Grignon, et al., Nucl. Instrum. Methods Phys. Res., Sect. A 571 (2007) 142–145.
[7] L.F. Masuner, et al., Appl. Radiat. Isot. 49 (4) (1998) 285–294.
[8] R.W. Baer, et al., Am. J. Physiol., Heart Circ. Physiol. 246 (3) (1984), H418–H434.
[9] A.P. Wehner, et al., Lung clearance of neutron activated Mount St. Helens volcanic ash in the rat, Environ. Res. 35 (1) (1984) 211–217.
[10] I. Mutsuo, K. Kazuhisa, Cosmogenic radionuclides in meteorites including recently fallen ones. Constraints on the exposure history of chondrites, Chikyu Kagaku 35 (1) (2001) 13–25 (in Japanese).
[11] R.D. Hichwa, et al., Nucl. Instrum. Methods Phys. Res., Sect. B 99 (1995) 804–806.
[12] F. Tarkanyi, et al., Beam Monitor Reactions, Charged Particle Cross-Section Database for Medical Radioisotope Production, IAEA-TECDOC-1211, IAEA, Vienna, Austria, 2001, http://www-nds.iaea.org/medical/S.
[13] J.N. Barrandon, et al., Nucl. Instrum. Methods Phys. Res., Sect. B 127 (2) (1975) 269–278.
[14] R.L. Brodzinski, et al., Phys. Rev. C 4 (1971) 1250–1257.
[15] D. Fink, et al., Nucl. Instrum. Methods B 52 (1990) 601–607.
[16] P. Jung, in: Conference on Nuclear Data for Science and Technology, Juelich, 1991, p. 352, Exfor D4058028.
[17] P. Kopecky, et al., Appl. Radiat. Isot. 44 (4) (1993) 687–692.
[18] R. Michel, et al., Nucl. Instrum. Methods B 129 (1997) 153–193.
[19] R. Michel, et al., J. Inorg. Nucl. Chem. 40 (11) (1978) 1845–1851.
[20] R. Michel, G. Brinkmann, J. Radioanal. Nucl. Chem. 59 (2) (1980) 467–510.
[21] F. Szelecsenyi, et al., Nucl. Instrum. Methods Phys. Res., Sect. B 174 (2001) 47–64.
[22] F. Tarkanyi, et al., in: Conference on Nuclear Data for Science and Technology, Juelich, 1991, p. 529, Exfor D4080003.
[23] S. Takacs, et al., Nucl. Instrum. Methods Phys. Res., Sect. B 188 (2002) 106–111.
[24] K. Zarie, et al., Radiochim. Acta 94 (12) (2006) 795–799.
[25] M.U. Khandaker, et al., Appl. Radiat. Isot. 67 (2009) 1348–1354.
[26] M.E. Bennett, et al., Nucl. Instrum. Methods Phys. Res., Sect. B 276 (2012) 62–65.
[27] A. Hermanne, et al., Nucl. Instrum. Methods Phys. Res., Sect. B 338 (2014) 31–41.
[28] E. Garrido, et al., Nucl. Instrum. Methods Phys. Res., Sect. B 383 (2016) 191–212.
[29] J.R. Walton, et al., J. Geophys. Res. 81 (10) (1976) 5689–5699.
[30] J.R. Walton, et al., J. Geophys. Res. 78 (28) (1973) 6428–6442.
[31] IAEA-EXFOR experimental nuclear reaction data base, http://www.nds.iaea.org/exfor.
[32] S. Parashari, et al., Nucl. Phys. A 978 (2018) 160–172.
[33] S. Parashari, et al., Nucl. Phys. A 979 (2018) 102–112.
[34] J.F. Ziegler, SRIM08, the Stopping and Range of Ions in Matter, http://www.srim.org/, 2008.
[35] NuDat 2.7β 2011, National Nuclear Data Center, Brookhaven National Laboratory, https://www.nndc.bnl.gov/nudat2/.
[36] Qtool: calculation of reaction Q-values and threshold, Los Alamos National Library, http://cdfe.sinp.msu.ru/services/calc_thr/calc_thr.html.
[37] R. Capote, et al., Nucl. Data Sheets 110 (2009) 3107.
[38] A.J. Koning, J.P. Declaroche, Nucl. Phys. A 713 (2003) 231.
[39] W. Hauser, H. Feshbach, Phys. Rev. 87 (1952) 366.
[40] C. Kalbach, Phys. Rev. C 33 (1986) 818.
[41] A. Gilbert, A.G.W. Cameron, Can. J. Phys. 43 (1965) 1446.
[42] W. Dilg, W. Schantl, H. Vonach, M. Uhl, Nucl. Phys. A 217 (1973) 269.
[43] A.V. Ignatyuk, K.K. Istekov, G.N. Smirenkin, Sov. J. Nucl. Phys. 29 (4) (1979) 450.
[44] A.V. Ignatyuk, J.L. Weil, S. Raman, S. Kahane, Phys. Rev. C 47 (1993) 1504.
[45] S. Goriely, S. Hilaire, A.J. Koning, Improved microscopic nuclear level densities within the HFB plus combinatorial method, Phys. Rev. C 78 (2008) 064307.
[46] S. Hilaire, M. Girod, S. Goriely, A.J. Koning, Temperature dependent combinatorial level densities with the D1M Gogny force, Phys. Rev. C 86 (2012) 064317.
[47] M. Blann, Phys. Rev. C 54 (1996) 1341.

[48] V.F. Weisskopf, D.E. Ewing, Phys. Rev. 57 (1940) 472.
[49] N. Bohr, J.A. Wheeler, Phys. Rev. 56 (1939) 426.
[50] M.B. Chadwick, P. Oblozinsky, Phys. Rev. C 50 (1994) 2490.
[51] J.R. Huizenga, L.G. Moretto, Annu. Rev. Nucl. Sci. 22 (1972) 427.